Surfaces and Interfaces 24 (2021) 101041

Contents lists available at ScienceDirect

Surfaces and Interfaces

journal homepage: www.sciencedirect.com/journal/surfaces-and-interfaces

Nano-shaping of gold particles on silicon carbide substrate from solid-state to liquid-state dewetting

F. Ruffino *, M.G. Grimaldi

Dipartimento di Fisica e Astronomia "Ettore Majorana" Università di Catania and MATIS CNR-IMM, via S. Sofia 64, 95123 Catania, Italy

ARTICLE INFO

Keywords:
Au
SiC
Solid state dewetting
Liquid state dewetting
Nano-shape

ABSTRACT

This work reports on the effect of annealing temperature on the size, shape and wetting of particles obtained on 4H-SiC substrate by the dewetting process of a deposited nanoscale-thick Au film, with focus on the difference between solid-state dewetting (below Au melting temperature) and liquid-state dewetting (above Au melting temperature).

After depositing nanoscale-thick Au film on the SiC substrate, annealings are perfomed so to induce the solid-state or liquid-state dewetting process of the film with the consequent formation of particles. Plan-view and cross-view scanning electron microscopy analyses are carried out to quantify the evolution of the average planar size and vertical size of the particles and of the average contact angle of the particles to the SiC surface versus the annealing temperature. These analyses allow us to extract quantitative information on the wetting behaviour of the particles on the SiC surface by calculating the adhesion work versus the annealing temperature. Energy dispersive x-ray analyses are, also, performed on the dewetted particles to analyze their composition in the various annealing conditions. Overall, we set a general framework connecting process parameters to the nano-shape of the dewetted particles towards specific shape design for selected applications.

1. Introduction

Silicon Carbide (SiC) is a semiconductor binary compound of silicon and carbon with peculiar properties such as ~~a~~ wide band gap, high phonon frequency, high thermal conductivity and breakdown voltage [1-6]. Due to these characteristics, SiC can be exploited in several technological applications ranging from electronics and optoelectronics to sensing and energy [1-6]. However, these applications require the use of metallic contacts to SiC and, from decades, metal/SiC diodes are exploited to design and produce high temperature and high power operating devices [1-6]. Hence, several methods were investigated for the controlled production of metal layers on SiC substrates. In addition, with the advent of nanomaterials and nanotechnologies, also the controlled production of metal nanostructures on SiC substrates acquired a relevant role to fabricate functional nanodevices with improved performances in electronics, energy, sensing applications [7-16], due to the synergistic combination of the properties of metals in nanoscale form [17-26] and of SiC. For example, Au and Ag nano-particles show strong optical resonances: under excitation by electromagnetic radiation, Au or Ag nano-particles can exhibit localized surface plasmon resonances due to the collective oscillations of conduction electrons [17-19]. An important consequence of the resonant excitation of localized surface plasmon resonances rely in selective photon absorption and enhancement of local electromagnetic fields near the nanostructure by orders of magnitude strongly depending on the nano-particles shape and size. Such a characteristic makes Au and Ag nanostructures very important in plasmonic solar cells [17-19, 27, 28] and in chemical and biological sensing exploiting the surface enhanced Raman spectroscopy effect [17-19, 29, 30]. In this regard, Au and Ag nanostructures produced on SiC substrates enhance the photoluminescence response of SiC [13, 16], give place to SERS effect for ultrasensitive molecules detection [11, 15, 16], enhance the SiC photocatalytic activity [14]. As a consequence, in order to enable solid-state technological applications, the main critical issue for the use of metal nanostructures is the development of simple, versatile, and low-cost methodologies for the fabrication of arrays of nanostructures with desired shape and size directly on surface, as the case of Au nano-particles on SiC substrate.Obviously, the detailed understanding of the basic microscopic mechanisms governing the involved processes in these methodologies is crucial in assuring the desired nanostructures control.

* Corresponding author.
E-mail address: francesco.ruffino@ct.infn.it (F. Ruffino).

https://doi.org/10.1016/j.surfin.2021.101041
Received 11 November 2020; Received in revised form 18 January 2021; Accepted 17 February 2021
Available online 22 February 2021

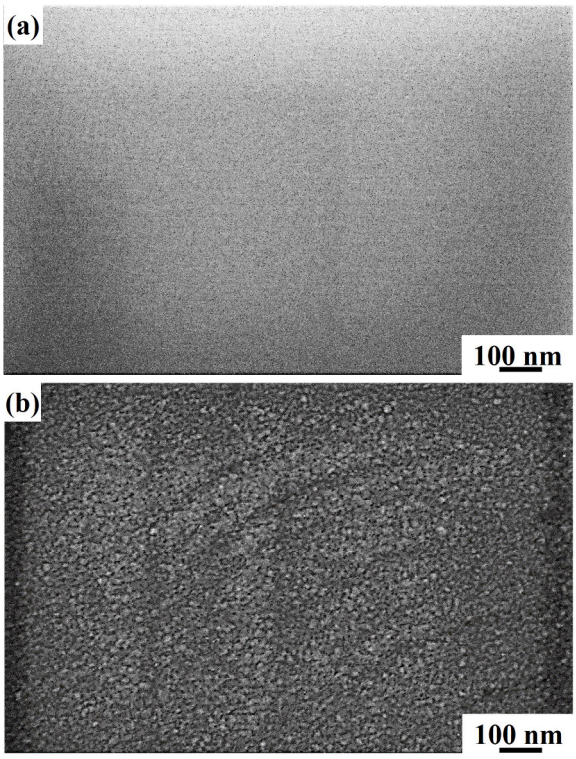

Fig. 1.. Representative SEM images of the bare SiC surface (a) and of the surface of the 50 nm-thick Au film deposited on the SiC substrate (b).

In particular, due to the importance acquired by the Au/SiC system [8-11, 31-36], we present here a dewetting-based approach to produce Au nano-particles directly on SiC surface and a study on their morphological, wetting, compositional properties using microscopic analysis as Scanning Electron Microscopy (SEM) and Energy Dispersive X-ray Spectroscopy (EDX).

In particular, we deposited a 50 nm-thick Au film on 4H-SiC substrate and we performed annealing processes of the system at temperature T=1173 K, 1253 K, below the Au melting temperature (1337 K), and T=1423 K, 1473 K, above the Au melting temperature, to induce solid-state or liquid-state dewetting of the Au film towards the formation of nanoscale particles.

Regarding the dewetting process, a metal film deposited on non-metal substrate in a metastable thermodynamic state and at sufficient high temperatures, even below the melting temperature of the material forming the film can spontaneously dewets forming island-like structures on the substrate surface. During this process the main driving force is the minimization of surface free energy on all interfaces and the resulting island size depends on various factors such as the initial film thickness and annealing temperature. Because this process can be activate at temperatures well below the T_{melt} of the material film, we can make a distinction between solid-state dewetting and liquid-state dewetting. Although both process lead to a formation of small particles starting from a thin film, the early stages of the process are quite different. The solid state dewetting [8, 37-40] process starts with holes formation on the surface. In this case an equilibrium relation is established between surface energies at the point in which grain boundaries and the substrate meet, forming a groove with a characteristic size, dependent on the initial film thickness and all the surface energies. If these grooves exceed a critical size, they will contact the substrate and holes will be formed. This process is more like to happen in stressed film, in which the critical size is reduced by stress energy transfer to the hole or by a grain thinning. In the next phase an edge retraction can be observed due to a curvature's gradient, that will lead to a net material flux from the rim to the central area, causing the formation of an hill like structure and the hole growth. Other than the temperature two other parameters play a key role on this process: the surface diffusivity and the film's free energy. From this point two growth trends can be observed [38, 39]: a) rim pinch-off, consisting in the formation of film's height oscillations with decreasing amplitude from the rim, forming valleys with increasing depth as the edges continues to retract. At a certain point the ditch's bottom will contact the substrate and a strand will forms; b) fingering instabilities, consisting in the rims edges break, forming an array of elongated, finger like structures. The cause of this different behaviour [37] can be found in the formation of equilibrium facets on the edge's front, which maintain a stability condition during the retracting process. In this case rim pinch off takes places. On the contrary, the absence of equilibrium facets can be attributed to unstable conditions during the edges retractions, leading to unstable rim's oscillations and to an array of fractal, elongated structures. In the final stage of dewetting all strands, formed thought rimn pinch-off or fingering instabilities, began to shows bottlenecks and breaks, forming islands as consequence of Rayleigh-Plateau instabilities [38, 39]. The film thickness and annealing temperature play an important role on the process [37-40]. In this regard, liquid phase dewetting process [41-43] is similar to the solid state one: the liquid film presents the holes formation, holes growth, filaments formation and filamnets break into liquid droplet on the substrate. For example, Krishna et al. [42, 43] showed that metal thin film with thickness less than 100 nm upon laser irradiation undergoes a spinodal dewetting, i.e. the dewetting process of a molten thin film presenting thickness fluctuations. So, the unstable

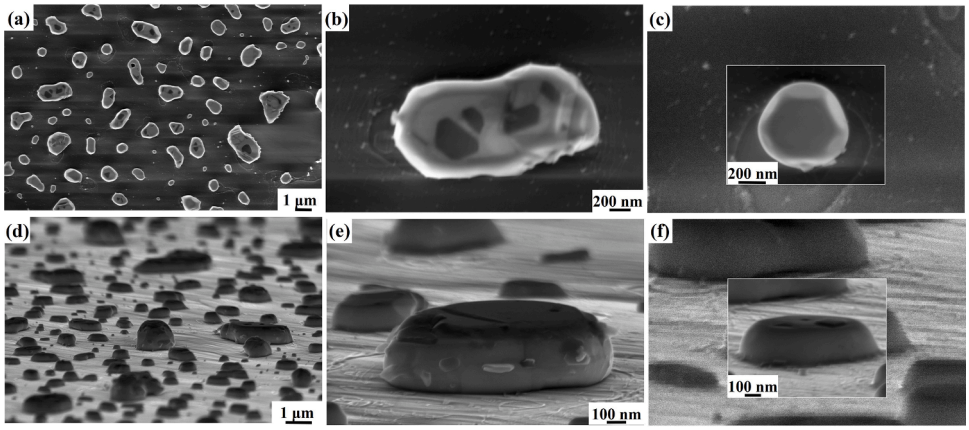

Fig. 2.. Representative SEM images of the Au particles obtained by the solid-state dewetting process of the 50 nm-thick Au film deposited on the SiC surface and annealed at 1173 K for 40 minutes: (a)-(c) plan-view images with different magnifications to highlight various features; (d)-(f) cross-view images with different magnifications to highlight various features.

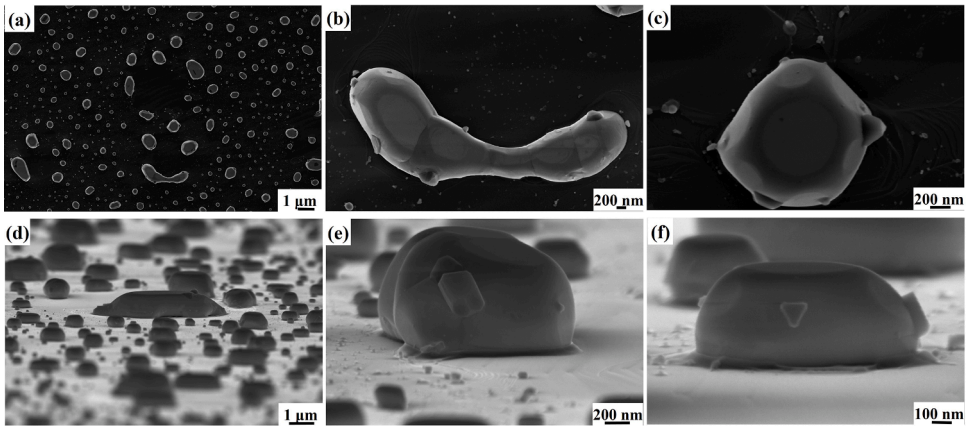

Fig. 3.. Representative SEM images of the Au particles obtained by the solid-state dewetting process of the 50 nm-thick Au film deposited on the SiC surface and annealed at 1253 K for 40 minutes: (a)-(c) plan-view images with different magnifications to highlight various features; (d)-(f) cross-view images with different magnifications to highlight various features.

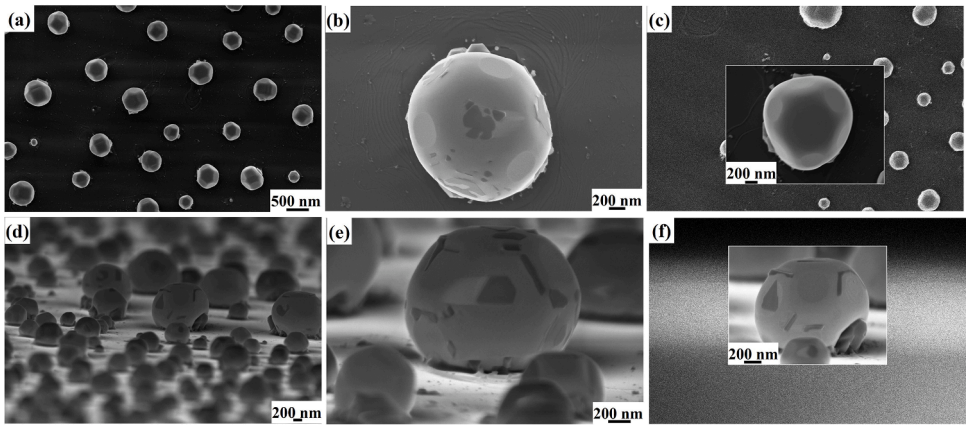

Fig. 4.. Representative SEM images of the Au particles obtained by the liquid-state dewetting process of the 50 nm-thick Au film deposited on the SiC surface and annealed at 1423 K for 40 minutes: (a)-(c) plan-view images with different magnifications to highlight various features; (d ₹)-(f) cross-view images with different magnifications to highlight various features.

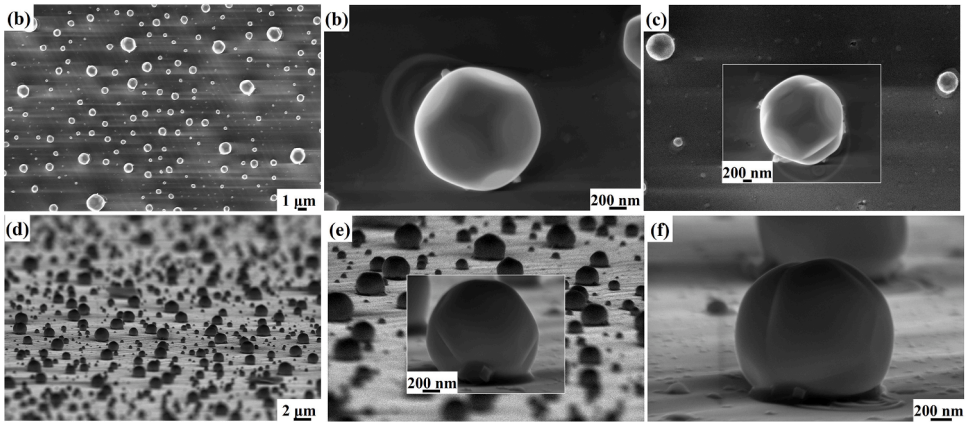

Fig. 5.. Representative SEM images of the Au particles obtained by the liquid-state dewetting process of the 50 nm-thick Au film deposited on the SiC surface and annealed at 1473 K for 40 minutes: (a)-(c) plan-view images with different magnifications to highlight various features; (d)-(f) cross-view images with different magnifications to highlight various features.

film's height leads to a change in the free energy and to the film's rupture and nanoparticles formation through Rayleigh-Plateau instabilities.

Therefore, in our case, at each annealing stage, SEM and EDX analysis were performed to image the step-by-step dewetting process of the Au film on the SiC substrate to draw information on the characteristics both of solid-state and liquid-state dewetting processes. The quantification of the dewetted particles average planar and vertical sizes and average contact angle was carried out for each annealing temperature and, hence, the temperature-dependent wetting properties of Au on SiC

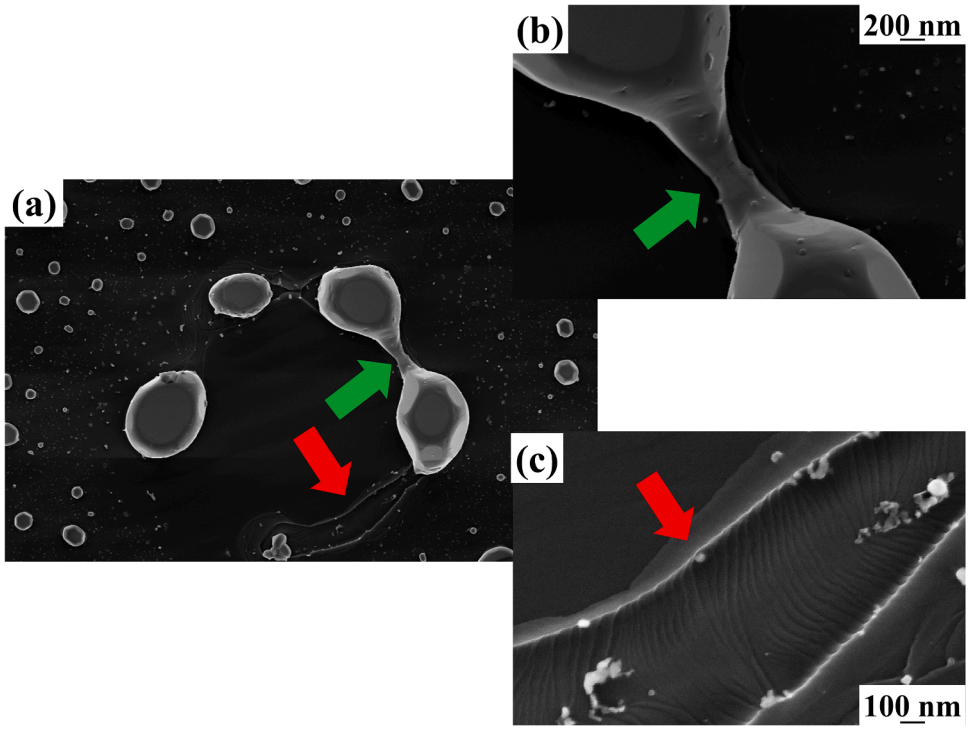

Fig. 6. Representative plan-view SEM images highlighting some specific features of the dewetting process leading to the formation of the Au particles (annealing at 1253 K).

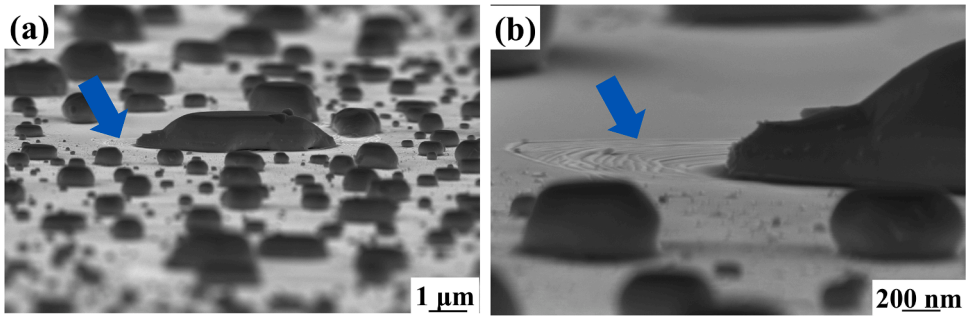

Fig. 7. Representative cross-sectional SEM images highlighting some specific features of the dewetting process leading to the formation of the Au particles (annealing at 1253 K).

were elucidated by the calcultion of the adhesion energies and interface energies. In this regard, the wetting behavior of solid or liquid Au on SiC has been previously reported [31-36, 44, 45] in studies, however, focused on bulk systems. These reports, studied the wetting of Au droplets on the SiC surface with the droplets having typical size of several microns since originating from the thermal process of deposited films with thickness larger than 1 μm. Hence, the studies presented in the this work aim to scale-down those previously reported for the macroscopic Au-SiC system to sub-micrometer and nanoscale range establishing an approach for the nano-shaping of Au particles on SiC. In particular, we set a general working framework connecting the annealing temperature to the nano-shape of the dewetted particles towards specific shape design for selected applications.

2. Experiment and methodology

Four samples have been synthesized starting from an Au thin film deposited using the sputtering technique. A sputter apparatus Emitech K550X was exploited, in which all the 4H-SiC substrates are located in the cathode, facing the Au source (purity of 99,999%), with a distance of 40 mm and using Ar flux with a pressure of 0,02 mbar, with a current of 50 mA for each samples. The entire process has been carried for 4 minutes resulting in the deposition of (50,0±2,5) nm-thick Au film on the 4H-SiC surface. The samples thickness is obtained by ex-situ Rutherford Backscattering Spectrometry (RBS) measurement, using 2 MeV $^4He^+$ backscattered at 165°.

The samples were thermally processed in nitrogen environment (flux of 2,5 liters/minute) fixing the annealing time t to 40 minutes and using the annealing temperature T=1173 K, 1253 K, below the Au melting temperature (1337 K), and =1423 K, 1473 K, above the Au melting temperature.

Scanning Electron Microscope (SEM) imaging was performed by using a Zeiss FEG-SEM Supra 25 Microscope (equipped with a Field Emission Gun emitter an In-Lens detector) both in plan-view and cross-view configurations. The SEM images were acquired by using the backscattered electrons, acceleration voltage for the electron beam of 5 kV, working distance of 3 mm. The images were analyzed by using the Gatan Digital Micrograph software to infer quantitative information: in particular, we evaluated the average planar and vertical sizes of the dewetted particles and their contact angle to the SiC substrate for each

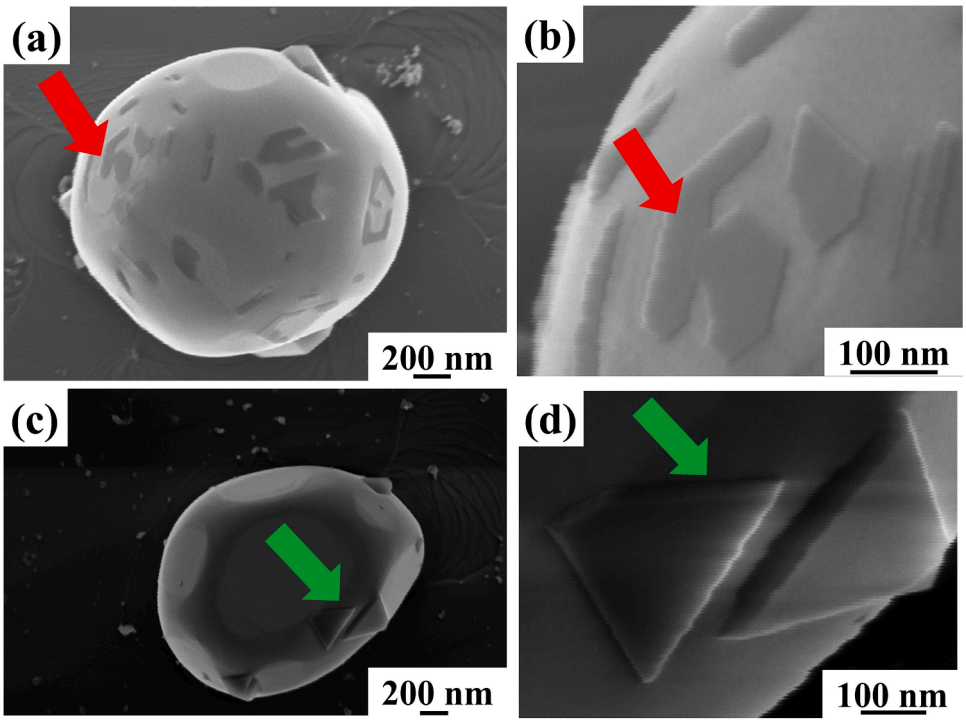

Fig. 8. Representative SEM images highlighting some specific features of the morphology of the dewetted particles ((a)-(b): plan-view images, annealing at 1473 K; (c)-(d): plan-view images, annealing at 1253 K).

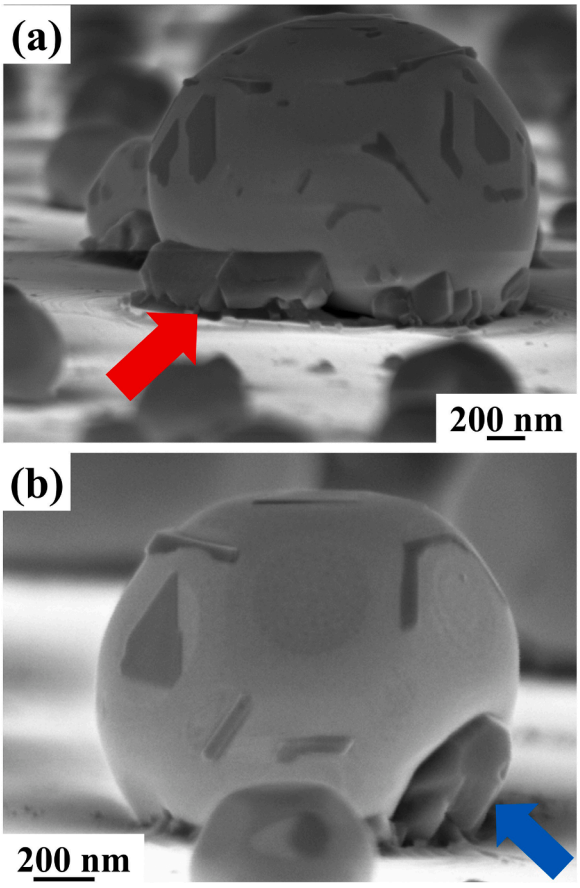

Fig. 9. Representative SEM images highlighting some specific features of the base of the dewetted particles, i. e. particles-substrate interface (cross-view images, annealing at 1423 K).

annealing temperature. To this end, the planar size of the single particles was measured, by the plan-view SEM images, as the equivalent disk diameter D by drawing the smallest circumference that contains the particle and taking the diameter. The vertical size H was, instead, evaluated by the cross-sectional SEM images, as the highest distance between the SiC substrate-particle interface and the top surface of the particle. The cross-sectional SEM images were, also, used to evaluate the contact angle θ_C as the angle between the direction of a line on the substrate surface and the direction of a line tangent to the particle surface in the point where it crosses the substrate surface. For each sample, a statistical population of, at least, 500 particles was considered to extract distributions for D, H, and θ_C, from which the mean values $<D>$, $<H>$, $<\theta_C>$ were evaluated (so as the corresponding standard deviations which were considered as the corresponding errors to the mean values). The wetting properties of the dewetted particles are quantified by the calculation of work of adhesion $W_{AD}=[1+\cos(<\theta_C>)]\gamma_{Au}$ after the experimental determination of $<\theta_C>$ for each annealing temperature and being γ_{Au} the Au surface energy.

Energy Dispersive X-ray (EDX) analyses were performed by using the Gemini Field Emission SEM (FE-SEM) Carl Zeiss SUPRA 25 Microscope equipped with an EDAX EDX detector, fixing the electron beam acceleration voltage to 25 kV, working distance of 8 mm, acquisition time of 240 s.

3. Results and discussions

Fig. 1(a) reports a representative SEM image of the bare SiC surface. Fig. 1(b) reports a representative SEM image of the surface of the 50 nm-thick Au film deposited on the SiC surface. In particular, from the image in Fig. 1(b) the surface of the 50 nm-thick Au film, if compared to the image in (a) for the bare SiC surface, appears to have a rough granular morphology, typical of the last stage for the Volmer-Weber growth mechanism for metal films on ceramic substrates [46-48]. In fact sputtered adsorbed Au atoms move on the SiC surface until they find an aggregationcenter, where the film begins to growth in the early stages of the process. In the Volmer-Weber growth mode, after the small nuclei

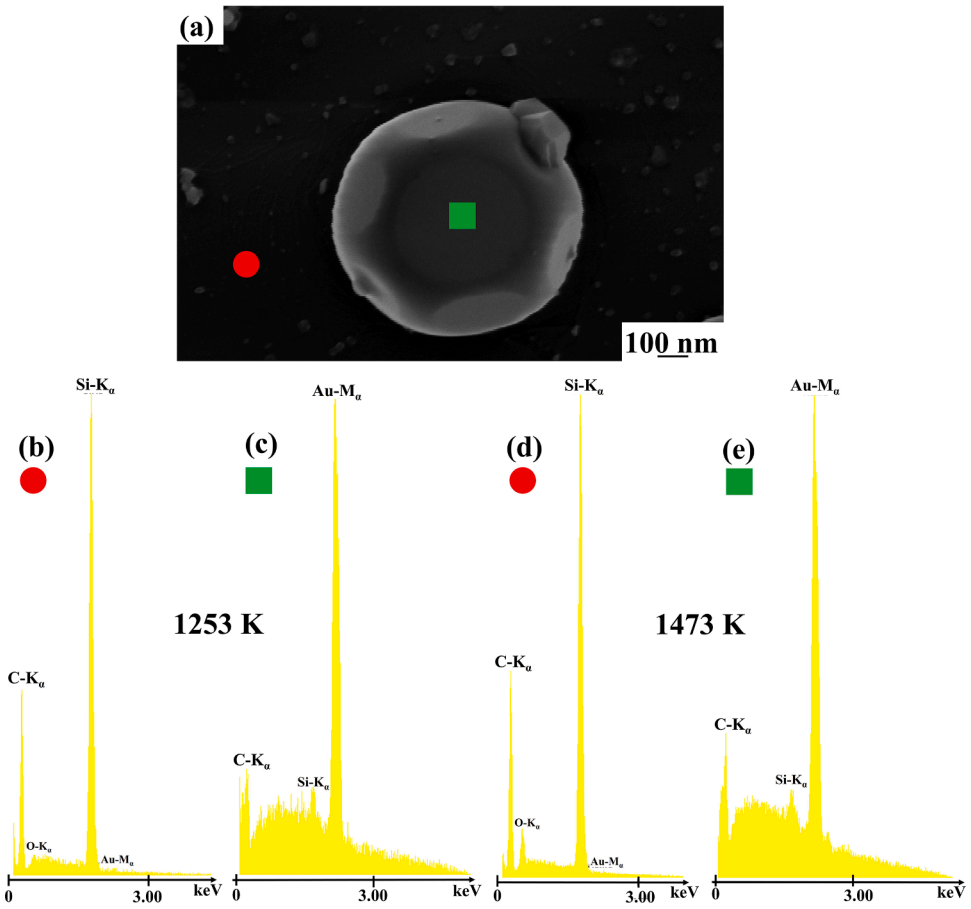

Fig. 10. (a) Plan-view SEM image of an isolated dewetted particle obtained at 1253 K; (b) EDX spectrum acquired in the position indicated by the red circle in (a), i. e. on the SiC substrate (outside the dewetted particle); (c) EDX spectrum acquired in the position indicated by the green square in (a), i. e. over the dewetted particle; (d) EDX spectrum acquired on a point over the bare SiC surface after 1473 K annealing of the 50 nm-thick Au film; (e) EDX spectrum acquired on a point over a dewetted particle obtained by the 1473 K annealing of the 50 nm-thick Au film.

formation, the nuclei continue togrowth becoming larger and higher giving origin to three-dimensional islands which, continuing to growth, percolate between them (i. e. over a certain critical size, these islands touch one another, forming grain boundaries and assuming a granular shape). At this late stage of growth, the film morphology is percolative, i. e. a worm-like structure originating from interconnected filaments. The holes in the film are, then, filled by further deposited atoms resulting in a granular rough film surface. Naming γ_{Au} the Au film-vapour surface energy, γ_{SiC} the SiC substrate-vapour surface energy, and $\gamma_{Au/SiC}$ the Ag film-SiC substrate interface energy, in the Volmer-Weber growth mode the relation $\gamma_{SiC}<\gamma_{Au}+\gamma_{Au/SiC}$ holds [48]. In fact, in this case, the film atoms are more bounded to each others than to the substrate (hence, the Volmer-Weber growth mode is typical for thin metal films deposited on non-metal substrates). Typical Au surface energy is of the order of 1,4 J/m^2 [49-54], while 4H-SiC surface energy has been calculated [55, 56] resulting in, about, 1,77 J/m^2.

After the Au film deposition, the annealing processes were carried out to induce the film dewetting both in solid-state and liquid-state by using annealing temperatures below (1173 K, 1253 K) and above (1423 K, 1473 K) the Au melting temperature (1337 K) and the consequent formation of particles on the SiC surface (Figs. 2-5).

We can clearly see that after processing the Au film/SiC sample at 1173 K and 1253 K (solid-state dewetting, Fig. 2 and Fig. 3, respectively) two dimensional (planarly elongated) islands are formed, i. e. with the planar size larger than the vertical size. In addition, equilibrium facets can be seen on the surface of the particles: in fact, the general equilibrium shape of the Au crystals consists of {111} and {100} facets connected by sharp edges to curved surfaces, i. e. to expose the crystals planes to which correspond the lower surface energies according to the FCC lattice structure [31-33,57]. This behaviour can be explained using the Wulff construction and the Winterbottom construction [48, 57]. On

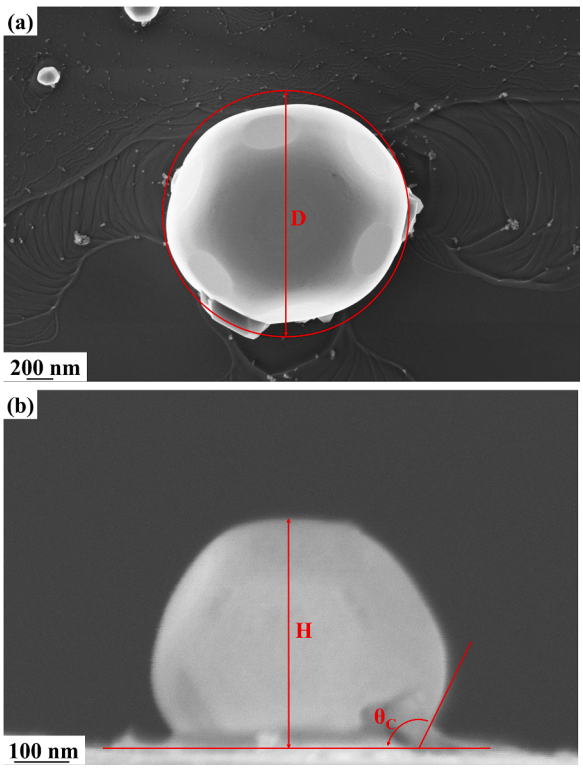

Fig. 11.. Representation of the method used for the measure of the planar size D (diameter) of the dewetted particles (a) and for the measure of the vertical size H (height) and contact angle θ_C (to the SiC substrate) of the dewetted particles (b).

the other hand, in the samples treated at 1423 K and 1473 K (liquid-state dewetting, Fig. 4 and Fig. 5, respectively), the formed particles show an almost spherical shape (planar size≈vertical size) and, also, they expose the characteristics {111} and {100} equilibrium facets. In any case, it can be easily recognized that the particles are homegeneously distributed over all the SiC surface and present a high dispersion in the planar and vertical sizes, being present, in each sample, very small particles and very large particles (this is characteristic of the stochastic nature of the dewetting process). Another feature that jumps out, comparing samples obtained by solid-state and liquid-state dewetting, is the different contact angle at the particles-substrate interface, as evident by comparing the cross-sectional SEM images from Fig. 2 to Fig. 5, corresponding to the various annealing temperatures. While the particles in the two samples obtained by solid-state dewetting (1173 K and 1253 K annealed) show a better wettability on the SiC surface, i. e. lower contact angle, instead the two samples obtained by liquid-state dewetting (1423 K and 1473 K annealed) exhibit particles with lower wettability (higher contact angle). In the following we will analyze quantitatively, the wetting behaviour of the dewetted particles to the SiC surface. As a starting point, we here anticipate that the wetting behaviour, as quantified by the contact angle θ_C (for its defition see Fig. 11(b)), is established by the combination of the γ_{Au}, γ_{SiC}, $\gamma_{Au/SiC}$ energies according to the Young's law [48]and lower θ_C higher the wetting of the particles.

$$\cos(\theta_C) = (\gamma_{SiC} - \gamma_{Au})/\gamma_{Au/SiC} \quad (1)$$

Figs. 6-9 report some further SEM images to highlight some features of the dewetting process leading to the formation of the particles and to highlight some features of the dewetted particles.

The first example is reported both in Fig. 6 and in Fig. 7. In particular, Fig. 6(a)-(c) report plan-view images of the effect of the 1253 K annealing on the Au film. In each image, the arrows indicate some specific feature. In (a), some big particles organized in a nearly circular spatial disposition can be observed. They originate from the breaking of an unstable filament (which originated from the coalescence of holes in the Au film). This can be recognized, as indicated by the green arrow, by observing (see the enlargement in (b)) the two big particles just connected by a residual filament: the further temporal evolution of the dewetting process (by increasing the annealing time) would lead to the shrinking of the filament diameter (with the corresponding increase of the particles size, i. e. mass transfer from the connecting filament to the particles) till to the complete filament rupture. In addition, the red arrow indicates (see the enlargement in (c)) the residual signature of the mass transfer, on the SiC surface, towards one of the particles. Similarly, Fig. 7 (a)-(b) report cross-view images of the effect of the 1253 K annealing on the Au film: the enlargement (b) of (a), as indicated by the blue arrow, clearly shows the signature, on the substrate surface, of the metal retraction (see the almost circular lines on the substrate surface) towards the formation of the particles (so to minimize the total surface energy of the system).

The second example is reported in Fig. 8: the figure shows SEM images highlighting some specific features of the morphology of the dewetted particles with (a)-(b) reporting plan-view images of the particles obtained after the annealing at 1473 K and (c)-(d) reporting plan-view images obtained after annealing at 1253 K. On the surface of the particles, some darker regions can be recognized and presenting regular geometries. In particular, (b) is an enlargement on the surface of the particle shown in (a) and (d) is an enlargement on the surface of the particle shown in (c). To infer the nature of these darker regions, we have to consider that the SEM images are acquired by using the backscattered electrons which are produced by elastic interactions of beam electrons with nuclei of atoms in the sample [58]. The images deriving by the backscattered electrons show characteristics of atomic number contrast, i.e., high average Z appear brighter than those of low average Z [58]. So, this is an indication of the fact that both solid-state and liquid-state dewetted particles are formed, in addition to Au (brighter regions of the surface of the particles), also by some contaminations with lower atomic number with respect to Au, possibly C and/or Si arising from the interaction with the SiC substrate. We observe that similar results were obtained by Ressel et al. [59] regarding the liquid-state dewetting of Au on Si substrate: in this case, the authors recognized the darker regions on the dewetted particles as precipitated Si.

The third example is reported in Fig. 9: the figure shows SEM images highlighting some specific features of the base of the dewetted particles, i. e. particles-substrate interface with (a)-(b) reporting cross-view images after annealing at 1423 K. The features highlighted by the arrows could indicate both signatures of the original retracted filament from which the particle originated and/or a particle-substrate reaction.

Regarding the elemental composition of the dewetted particles, we performed compositional analysis by acquiring EDX spectra on single particles for each annealing temperatures. Representative results are reported in Fig.10: as an example, (a) reports the plan-view SEM image of an isolated dewetted particle obtained at 1253 K, (b) reports the EDX spectrum acquired in the position indicated by the red circle in (a), i. e. on the SiC substrate (outside the dewetted particle) and (c) reports the EDX spectrum acquired in the position indicated by the green square in (a), i. e. over the dewetted particle. Similarly, (d) reports the EDX spectrum acquired on a point over the bare SiC surface after annealing the Au/SiC system at 1473 K (SEM image not shown) and (e) reports the EDX spectrum acquired on a point over a dewetted particle obtained after annealing the Au/SiC system at 1473 K (SEM image not shown). In all the EDX spectra acquired directly on the SiC surface (i. e. outside the dewetted particles) the characterstic intense lines corresponding to Si and C are clearly visible. In addition, the line corresponding to O can be recognized and whose intensity increases by increasing the annealing temperature, hence indicating an involuntary surface oxidation of the SiC surface. However, at the temperatures of 1173 K, 1253 K and 1423 K the O line can be considered only as a very small contamination (the O line in the spectrum in Fig. 10(b) is representative for these three

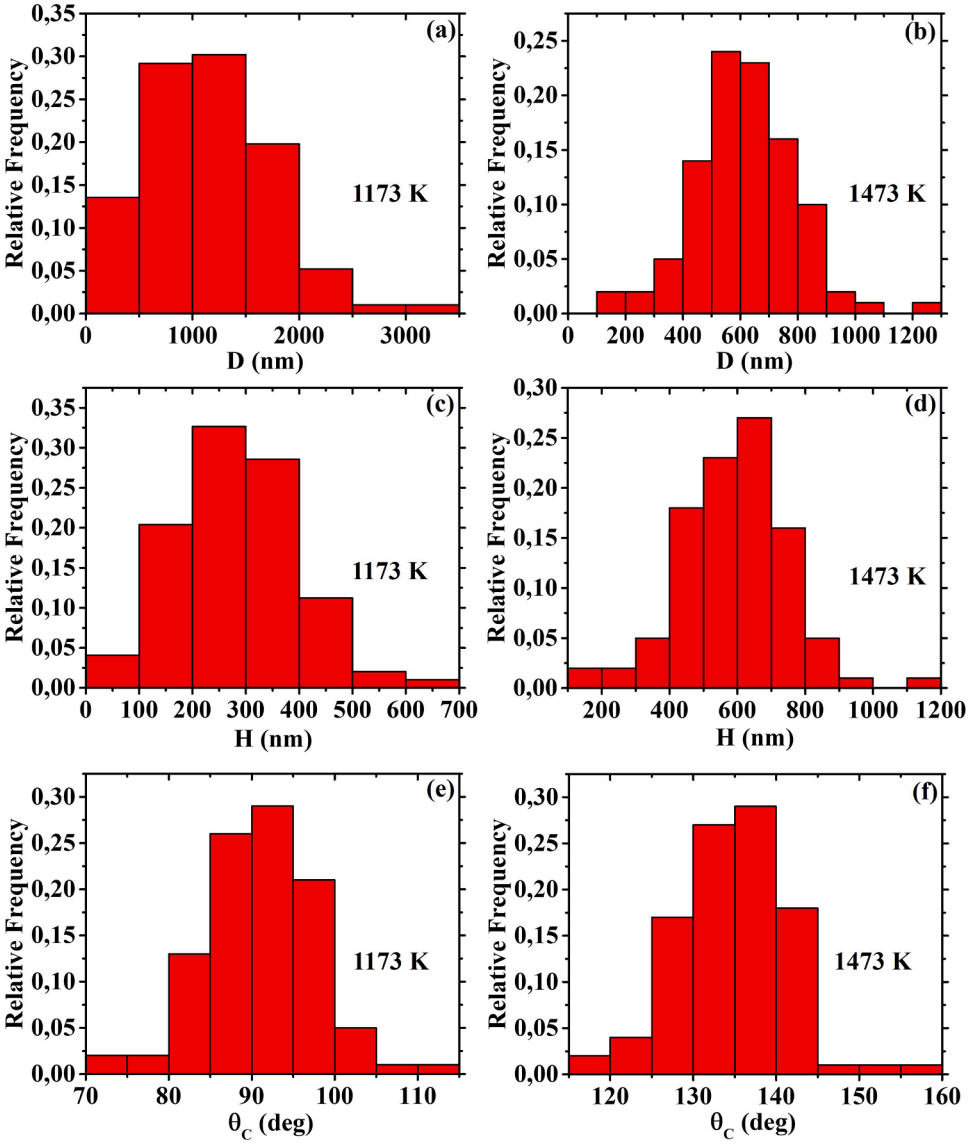

Fig. 12. Examples of histograms presenting: (a)-(b) the planar size (D) distributions measured (by the plan-view SEM images) for the dewetted particles on the SiC surface as obtained by the 1173 K annealing ((a)) and by the 1473 K annealing ((b)); (c)-(d) the vertical size (H) distributions measured (by the cross-view SEM images) for the dewetted particles on the SiC surface as obtained by the 1173 K annealing ((c)) and by the 1473 K annealing ((d)); (e)-(f) the contact angle (θ_C) distributions measured (by the cross-view SEM images) for the dewetted particles on the SiC surface as obtained by the 1173 K annealing ((e)) and by the 1473 K annealing ((f)).

samples). However, only at the annealing temperature of 1473 K the O line slightly increases in intensity (spectrum in Fig. 10(d)) indicating the occurring, at this temperature, of a slight oxidation of the SiC surface due to residual O_2 in the annealing chamber, as typical for SiC annealing at high temperature [60-62]. Regarding the EDX spectra acquired over the dewetted particles (see Fig. 10(c) and 10(e) for an example), all the spectra exhibit a very intense Au peak and Si and C peaks with lower intensities: hence, we conclude that the dewetted particles obtained for each annealing temperature (so, both by solid-state and liquid-state dewetting) are formed, mainly, by Au with some C and Si contamination arising from the interaction with the underlaying SiC interface. Generally, the Au-SiC system is classified as a non-reactive system [36], however the degree of reactivity is strongly dependent on temperature and Au and Si concentrations. In any case, the Au-SiC system is more less reactive if compared, for example, to the Ti-SiC or Ni-SiC systems [36]. The non-reactivity of the Au-SiC system means that [36] there are almost no chemical reactions between the metals and SiC under the standard experimental conditions. However, depending on the annealing temperature and Si concentration, for example, Si chemisorption at the Au/SiC interface [44] or electronic interactions between Au and Si atoms with the SiC substrate [45] can occur. Based on our results, and following some results by Naidich et al. [45], we can conclude that in our conditions (50 nm-thick Au and the chosen annealing temperatures), Au at high temperature can decompose SiC due to Au-Si interaction. Au-Si interatomic bonds are strong enough (in fact, the temperature required to dissolve Au in Si is high, corresponding to 28 KJ/mol). This description is supported by the fact that in some works a number of Au-Si compounds such as Au_nSi were found at high rapid cooling of Au-Si melts [63, 64]. So, when the interaction between Au-SiC takes place, the compounds Au-Si are formed and free carbon is precipitated which can be observed on the surface of the droplets on the SiC surface.

Now, we present the quantitative analysis. First of all, Fig. 11 reports an example of the use of the plan-view and cross-sectional SEM images to determine D, H and θ_C for a specific particle, as qualitatively described in the "Experiment and Methodology" section. Then, proceeding to the statistical analysis, Fig. 12 shows the resulting histograms, presenting in (a)-(b) the planar size (D) distributions measured for the dewetted particles on the SiC surface as obtained by the 1173 K annealing ((a)) and by the 1473 K annealing ((b)); in (c)-(d) the vertical size (H) distributions measured for the dewetted particles on the SiC surface as obtained by the 1173 K annealing ((c)) and by the 1473 K annealing ((d)); in (e)-(f) the contact angle (θ_C) distributions measured for the dewetted particles on the SiC surface as obtained by the 1173 K annealing ((e)) and by the 1473 K annealing ((f)). The obtained

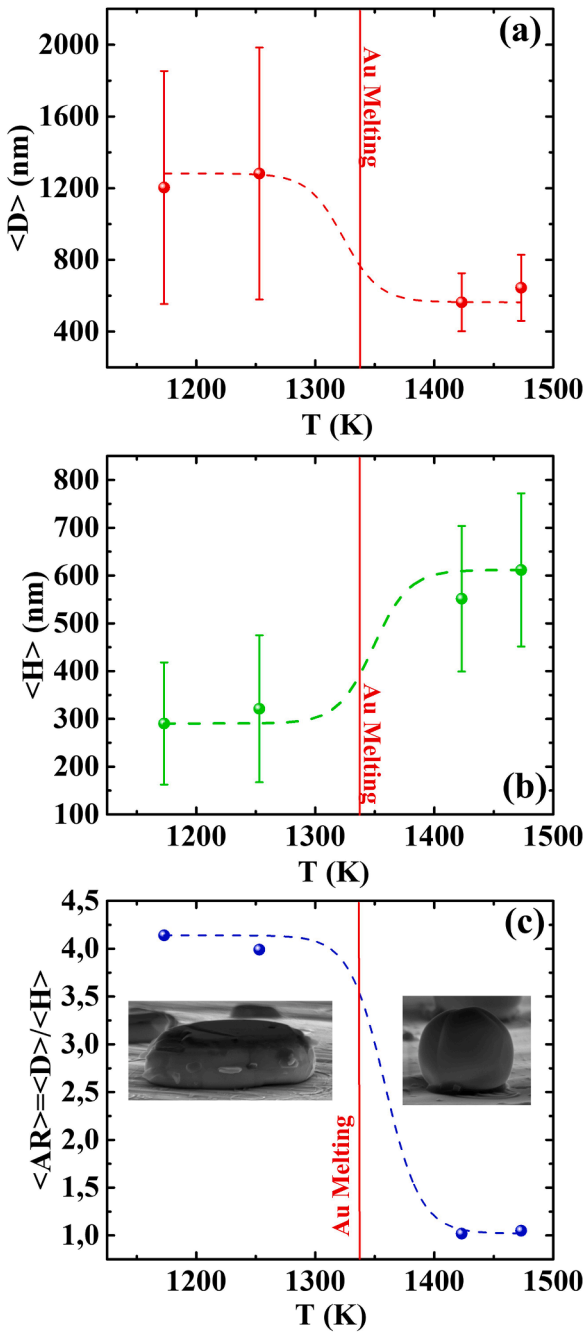

Fig. 13. (a) Plot of the average planar size (<D>) of the dewetted particles versus the annealing temperature, with the specific indication of the Au melting temperature (vertical red line) separating solid-state dewetting from liquid state dewetting; (b) Plot of the average vertical size (<H>) of the dewetted particles versus the annealing temperature, with the specific indication of the Au melting temperature (vertical red line) separating solid-state dewetting from liquid state dewetting; (c) Plot of the average aspect ratio (<AR>=<D>/<H>) of the dewetted particles versus the annealing temperature, with the specific indication of the Au melting temperature (vertical red line) separating solid-state dewetting from liquid state dewetting. In (c) the insets reports representative cross-view SEM images indicating the typical shape of the dewetted particles obtained by solid-state dewetting ((<AR>)>1) and by liquid-state dewetting ((<AR>)≈1).

distributions were used to extract the mean values <D>, <H>, <θ_C>. Therefore, Fig. 13 reports in (a) the plot of the average planar size (<D>) of the dewetted particles versus the annealing temperature, in (b) the plot of the average vertical size (<H>) of the dewetted particles

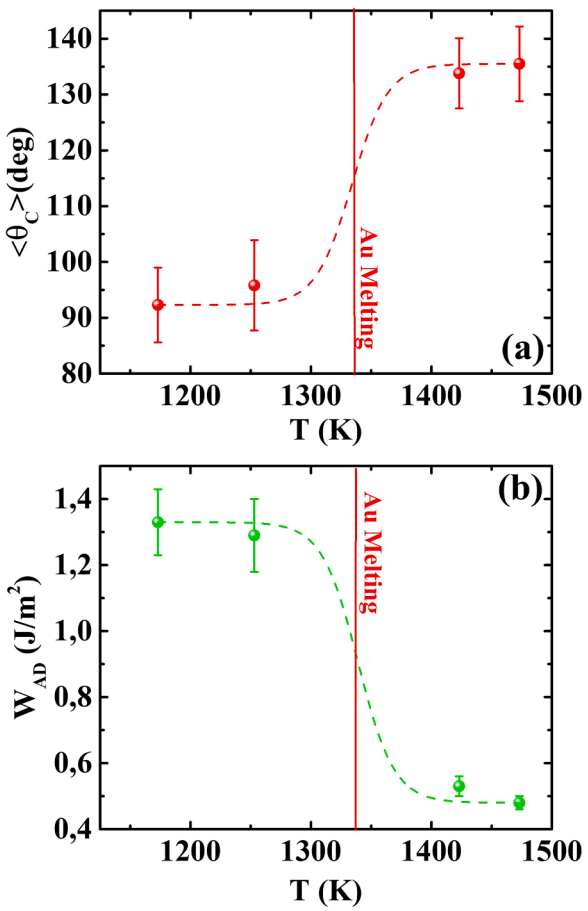

Fig. 14. (a) Plot of the average contact angle (<θ_C>) of the dewetted particles versus the annealing temperature, with the specific indication of the Au melting temperature (vertical red line) separating solid-state dewetting from liquid state dewetting; (b) Plot of the calculated work of adhesion (W_{AD}) of the dewetted particles versus the annealing temperature, with the specific indication of the Au melting temperature (vertical red line) separating solid-state dewetting from liquid state dewetting

Table 1
This table summarizes the average contact angle <θ_C> of the dewetted Au nanostructures on the SiC surface as measured by the cross-sectional SEM images, the calculated adhesion work W_A for the Au nanostructures on the SiC surface, and the calculated interface energy between Au and SiC for each annealing temperature determining the Au film dewetting process.

Sample	<θ_C> (deg.)	γ_{Au} (J/m^2)	W_A (J/m^2)	$\gamma_{Au/SiC}$ (J/m^2)
Au/SiC 1173 K	92,3±6,7	1,390 [45]	1,33±0,10	1,83±0,13
Au/SiC 1253 K	95,8±8,1	1,430 [45]	1,29±0,11	1,91±0,16
Au/SiC 1423 K	121,8±6,3	1,113 [41]	0,53±0,03	2,35±0,13
Au/SiC 1473 K	124,5±5,7	1,109 [41]	0,48±0,02	2,40±0,12

versus the annealing temperature, in (c) the plot of the average aspect ratio (<AR>=<D>/<H>) of the dewetted particles versus the annealing temperature. In each plot the vertical red line indicates the Au melting temperature and, hence, separates solid-state dewetting from liquid state dewetting. In (c) the insets reports representative cross-view SEM images indicating the typical shape of the dewetted particles obtained by solid-state dewetting ((<AR>)>1) and by liquid-state dewetting ((<AR>)≈1). For the annealing temperatures T=1173 K, 1253 K (solid-state dewetting) the average planar size is, about, constant to <D>≈1240 nm, the average vertical is, about, constant to <H>≈300 nm, the average aspect ratio is, about, constant to <AR>≈4,1. Increasing the annealing temperature above the Au metling

temperature, i. e. passing to liquid state dewetting, the average planar size decreases to the, about, constant value <D>≈600 nm, the average vertical size increases to the, about, constant value <H>≈580 nm, and the average aspect ratio decreases to the, about, constant value <AR>≈1. So, as indicated by the insets in Fig. 13(c), the dewetted particles evolve, by increasing the annealing temperature from below to above the Au metling temperature, from two-dimensional islands ((<D>)>(<H>)) to spherical particles ((<D>)≈(<H>)). This particles reshaping towards the spherical shape is driven by the minimization of the surface energy activated by the Au atom self-surface diffusion. At the higher temperatures, in particular in the liquid phase, the Au mobility is very high promoting the surface diffusion of the Au atoms from the high curvature (i.e., tip) to the low curvature (i.e., waist) regions of the particles [65, 66]. Then, Fig. 14(a) presents the evolution of the average contact angle (<θ_C>) of the dewetted particles versus the annealing temperature, with the specific indication of the Au melting temperature (vertical red line) separating solid-state dewetting from liquid state dewetting. We can observe that, increasing the annealing temperature from solid-state to liquid-state dewetting, in correspondence of the reshaping of the particles from two-dimensional islands to spherical particles, the average contact angle increases from, about, the constant value 94° to the, about, constant value 135° indicating a strong decrease of the wetting properties of Au to SiC by increasing the temperature above the Au melting temperature. The work of adhesion for the dewetted particles on the SiC substrate is defined as $W_{AD}=\gamma_{Au}+\gamma_{SiC}-\gamma_{Au/SiC}$ and, by eq.(1), it is directly related to the experimental determined average values for <θ_C>, as it results $W_{AD}=[1+\cos(<\theta_C>)]\gamma_{Au}$.

To summarize, Table1 reports, for each annealing temperature, the determined values for the average contact angle of the particles to the SiC surface and the values of the surface energy γ_{Au} for Au so as extracted by literature works. In this regard, γ_{Au} shows a dependence on temperature [49-54], decreasing by increasing temperature and, in particular, showing a drastic decrease passing from solid-state to liquid state phase for Au. By using the literature values for γ_{Au} reported in Table 1, by using the experimental derived values for the average contact angle θ_C and by using $W_{AD}=[1+\cos(<\theta_C>)]\gamma_{Au}$, for each annealing temperature the value of the work of adhesion W_{AD} for the dewetted particles to the SiC surface was calculated as reported in Table 1 and in Fig. 14(b): by increasing the annealing temperature from below to above Au melting temperature, in correspondence of the increase of the average contact angle of the particles, the work of adhesion decreases from, about, the constant value 1,31 J/m^2 (below melting) to, about, the constant value 0,51 J/m^2. In addition, by using, for the surface energy of SiC, the literature calculated value γ_{SiC}=1,77 J/m^2 [55, 56] (the surface energy of SiC is difficult to measure, however this calculated value is often used in a wide temperature range) and by using $W_{AD}=\gamma_{Au}+\gamma_{SiC}-\gamma_{Au/SiC}$, with the evaluated values for the adhesion work W_A, the values for the Au/SiC interfacial energy were calculated and reported in Table 1: according tho these assumptions and these calculations, the Au/SiC interfacial energy increases from 1,83 J/m^2 at 1173 K to 2,40 J/m^2 at 1473 K.

To conclude, we mention that the wetting of solid or liquid bulk Au on SiC has been investigated in some previous reports [31-36, 44, 45] and has been demonstrated to be poor, with reference to annealing of deposited films with thickness typically larger than 1 μm and originating droplets of several microns in size. Wang and Wynblatt [31-36] studied the solid-state dewetting of 1 μm-thick Au film deposited on α-SiC in various conditions. Generally, they obtained 10 μm-sized spherical Au droplets on the SiC surface and the key result is that pure Au exhibits a contact angle of 133° on the SiC substrate at 1123 K and a corresponding work of adhesion of 0.445 J/m^2. In their experiments, no C or Si contaminations of the Au droplets were detected. Drevet et al. [44] reported a contact angle 138° for liquid Au on α-SiC at 1373 K, which agrees well with the results obtained by Naidich et al. [45] at 1423 K. However, Drevet et al. [44] also observed an improved wetting of liquid Au on α-SiC by alloying Au with Si. They measured a decrease in contact angle from greater than 90° to less than 90° after the addition of Si to Au, and explained this result by invoking adsorption of Si at the Au/SiC interface, driven by the formation of a strong chemical bond at the interface. In this regard, futhermore, Naidich et al. [45]investigated the influence of silicon content and temperature on the wetting of Au–Si/SiC system, obtaining contact angles, at temperatures ranging from 1373 to 1773 K, varying as a function of Si content, with pronounced minima at about 5° at 1500 K for Si relative concentration of 0,3. In this case, the authors attributed the presence of a minimum in the contact angle to the electronic interactions between Au and Si atoms with the SiC substrate: Au–Si interactions in the liquid phase should strengthen the Si-SiC bonds with a transition of valence electrons towards Si atoms. Thus, more-covalent bonds can be established between Si atoms in the alloy and those in the substrate, leading, as a result, to an increased wettability. Nogi and Ogino [67] found even lower values of the contact angle (118° at 1373 K and 110° at 1453 K) of Au macroscopic bond on α-SiC.

Overall, the studies and results reported by us in the present work scale-down those previously reported for the macroscopic Au-SiC system to sub-micrometer and nanoscale range establishing an approach for the nano-shaping of Au particles on SiC surface for designed nanotechnology-related applications ranging from plasmonics to sensing.

4. Conclusion

Different nano-shaped particles were obtained on the surface of 4H-SiC by depositing a nanoscale-thick Au film and promoting, by annealings, the film solid-state or liquid-state dewetting process.

Morphological analyses using SEM images were carried out with the following results:

1) the 1173 K- and 1253 K-annealed samples (i.e. solid-state dewetting) present a formation of two-dimensional islands with the average planar size larger than the average vertical size and an average aspect ratio of, about, 4,1. For these samples, in particular, the average planar size is, about, constant to <D>≈1240 nm, the average vertical is, about, constant to <H>≈300 nm;
2) the 1423 K- and 1473 K-annealed samples (i.e. liquid-state dewetting) present a formation of three-dimensional spherical with the average planar size very similar to the average vertical size, i. e. with an average aspect ratio of, about, 1. For these samples, in particular, the average planar size is, about, constant to <D>≈600 nm, the average vertical is, about, constant to <H>≈580 nm;
3) In any case, the general shape of the Au particles consists of sharply defined facets at {100} and {111} orientations;
4) the dewetted particles are formed by Au with some inclusions of C and Si due to the Au interaction with the SiC substrate during the annealing processes;
5) Contact angle measurements for the dewetted particles on the SiC surface underline different wetting properties for solid-state and liquid-state dewetted particles. In particular, the solid-state dewetted particles show an average lower contact angle, about 94°, than the liquid-state contact angle, about 135° indicating a decrease in the wetting of the particles to SiC by increasing the temperature above the Au melting temperature;
6) the wetting nature of the particles to the SiC surface was quantified by the calculation of the work of adhesion which resulted about 1,31 J/m^2 below the Au melting temperature and about 0,51 J/m^2 above the Au melting temperature.

Data availability

The raw/processed data required to reproduce these findings cannot be shared at this time as the data also forms part of an ongoing study.

Declaration of Competing Interest

The authors declare that they have no known competing financial interests or personal relationships that could have appeared to influence the work reported in this paper.

Acknowledgments

This work was supported by the project "Programma di ricerca di ateneo UNICT 2020-22 linea 2" of the University of Catania-Italy and by the project PON MIUR ADAS+ (ARS01_00459).

References

[1] S.E. Saddow, A. Agarwal, Advances in Silicon Carbide Processing and Applications, Artech House Inc., Norwood, 2004.
[2] T. Kimoto, J.A. Cooper, Fundamentals of Silicon Carbide Technology-Growth, Characterization, Devices, and Applications, Wiley, Singapore, 2014.
[3] M. Shur, S. Rumyantsev, M. Levinshtein, SiC Materials and Devices, vol. 1 and vol. 2, World Scientific Publishing, Singapore, 2007.
[4] L.M. Porter, R.F. Davis, A critical review of ohmic and rectifying contacts for silicon carbide, Mater. Sci. Eng. B 34 (1995) 83–105.
[5] K. Zekentes, K. Vasilevskiy, Advancing Silicon Carbide Electronics Technology I-Metal Contacts to Silicon Carbide: Physics, Technology, Applications, Materials Research Forum LLC, USA, 2018.
[6] P. Friedrichs, T. Kimoto, L. Ley, G. Pensl, Silicon Carbide-Power Devices and Sensors, Vol. 2, Wiley, Weinheim, 2010.
[7] S. Yun, L. Wang, C. Zhao, Y. Wang, T. Ma, A new type of loss-cost counter electrode catalyst based on platinum nanoparticles loaded onto silicon carbide (Pt/SiC) for dye-sensitized solar cells, Physical Chemistry Chemical Physics 15 (2013) 4286–4290.
[8] F. Ruffino, M.G. Grimaldi, Formation of patterned arrays of Au nanoparticles on SiC surface by template confined dewetting of normal and oblique deposited nanoscale films, Thin Solid Films 536 (2013) 99–110.
[9] F. Ruffino, M.G. Grimaldi, F. Giannazzo, F. Roccaforte, V. Raineri, Size-dependent Schottky barrier height in self-assembled gold nanoparticles, Appl. Phys. Lett. 89 (2006), 243113.
[10] K. Fukuda, N. Yamada, D. Sadakane, S. Sakamoto, N. Fukumuro, S. Yae, Displacement deposition of gold nanoparticles and electroless deposition of nickel films on silicon-carbide (4H-SiC) wafers, Int. J. Surf. Eng. Coat. 95 (2017) 203–206.
[11] N. Bhalla, A. Jain, Y. Lee, A.Q. Shen, D. Lee, Dewetting metal nanofilms-effect of substrate on refractive index sensitivity of nanoplasmonic gold, Nanomaterials 9 (2019) 1530.
[12] M.M. Giangregorio, B. Dastmalchi, A. Suvorova, G.V. Bianco, K. Hingerl, G. Bruno, M. Losurdo, Effect of interface energy and electron transfer on shape, plasmon resonance and SERS activity of supported surfactant-free gold nanoparticles, RSC Adv 4 (2014) 29660.
[13] Y. Wei, W. Xin-Zhan, D. Wan-Lei, L. Wan-Bing, L. Yu-Mei, F. Guang-Sheng, Surface plasmon enhanced photoluminescence in amorphous silicon carbide by adjusting Ag island film sizes, Chin. Phys. B 22 (2013), 057804.
[14] S. Adhikari, N.K. Eswar, S. Sangita, D. Sarkar, G. Madras, Investigation of nano Ag-decorated SiC particles for photoelectrocatalytic dye degradation and bacterial inactivation, J. Photochem. Photobiol. A 357 (2018) 118–131.
[15] M.K. Kuntumalla, V.V.S.S. Srikanth, S. Ravulapalli, U. Gangadharini, H. Ojha, N. R. Desai, C. Bansal, SERS activity of Ag decorated nanodiamond and nano-β-SiC, diamond-like-carbon and thermally annealed diamond thin film surfaces, Phys. Chem. Chem. Phys. 17 (2015) 21331–21336.
[16] K. Kamakshi, K.C. Sekhar, A. Almeida, J. Agostinho Moreira, M.J.M. Gomes, Surface plasmon resonances-coupled photoluminescence and resistive switching behaviour of pulsed laser-deposited Ag:SiC nanocermet thin films, Plasmonics 10 (2015) 1211–1217.
[17] R.L. Johnston, J.P. Wilcoxon, Metal Nanoparticles and Nanoalloys, Elsevier, Amsterdam, 2012.
[18] Y. Xiong, X. Lu, Metallic Nanostructures—From Controlled Synthesis to Applications, Springer, New York, 2014.
[19] H.A. Atwater, A. Polman, Plasmonics for improved photovoltaic devices, Nature Materials 9 (2010) 205–213.
[20] M. Censabella, V. Torrisi, S. Boninelli, C. Bongiorno, M.G. Grimaldi, F. Ruffino, Laser ablation synthesis of mono- and bimetallic Pt and Pd nanoparticles and fabrication of Pt-Pd/graphene nanocomposites, Appl. Surf. Sci. 475 (2019) 494–503.
[21] V. Torrisi, F. Ruffino, Nanoscale structure of submicron-thick sputter-deposited Pd films: effect of the adatoms diffusivity by the film-substrate interaction, Surf. Coat. Technol. 315 (2017) 123–129.
[22] F. Ruffino, R. De Bastiani, M.G. Grimaldi, C. Bongiorno, F. Giannazzo, F. Roccaforte, C. Spinella, V. Raineri, Self-organization of Au nanoclusters on the SiO_2 surface induced by 200 keV-Ar^+ irradiation, Nucl. Instr. Meth. Phys. Res. B 257 (2007) 810–814.
[23] F. Ruffino, A. Pugliara, E. Carria, L. Romano, C. Bongiorno, G. Fisicaro, A. La Magna, C. Spinella, M.G. Grimaldi, Towards a laser fluence dependent nanostructuring of thin Au films on Si by nanosecond laser irradiation, Appl. Surf. Sci. 258 (2012) 9128–9137.
[24] D.K. Avasthi, Y.K. Mishra, D. Kabiraj, N.P. Lalla, J.C Pivin, Synthesis of metal-polymer nanocomposite for optical applications, Nanotechnology 18 (2007), 125604.
[25] Y.K. Mishra, D. Kabiraj, I. Sulania, J.C. Pivin, D.K. Avasthi, Synthesis and characterization of gold nanorings, J. Nanosci. Nanotechnol. 7 (2007) 1878–1881.
[26] Y.K. Mishra, R. Adelung, G. Kumar, M. Elbahri, S. Mohapatra, R. Singhal, A. Tripathi, D.K. Avasthi, Formation of Self-organized Silver Nanocup-Type Structures and Their Plasmonic Absorption, Plasmonics 8 (2013) 811–815.
[27] Yu.A. Akimov, W.S. Koh, K. Ostrikov, Enhancement of optical absorption in thin-film solar cells through the excitation of higher-order nanoparticle plasmon modes, Optic Express 17 (2009) 10195.
[28] Yu.A. Akimov, W.S. Koh, Resonant and nonresonant plasmonic nanoparticle enhancement for thin-film silicon solar cells, Nanotechnology 21 (2010), 235201.
[29] Z.–Y. Li, Metal Nanoparticles with Gain toward Single-Molecule Detection by Surface-Enhanced Raman Scattering, Nano Lett 10 (2010) 243–249.
[30] C. Matricardi, C. Hanske, J.L. Garcia-Pomar, J. Langer, A. Mihi, L.M. Liz-Marzan, Gold Nanoparticle Plasmonic Superlattices as Surface-Enhanced Raman Spectroscopy Substrates, ACS Nano 12 (2018) 8531–8539.
[31] Z. Wang, P. Wynblatt, The equilibrium form of pure gold crystals, Surf. Sci. 398 (1998) 259–266.
[32] Z. Wang, P. Wynblatt, Wetting and energetics of solid Au and Au-Ge/SiC interfaces, Acta Mater 46 (1998) 4853–4859.
[33] Z. Wang, P. Wynblatt, Alloying effects of Sn and Si on wetting and energetics of solid Au/SiC interfaces, Mater. Sci. Eng. A 259 (1999) 287–295.
[34] P. Wynblatt, The effects of interfacial segregation on wetting in solid metal-on-metal and metal-on-ceramic systems, Acta Mater 48 (2000) 4439–4447.
[35] C. Rado, S. Kalogeropoulou, N. Eustathopoulos, Bonding and Wetting in Non-Reactive Metal/SiC Systems: Weak or Strong Interfaces? Mater. Sci. Eng. A 276 (2000) 195–202.
[36] G.W. Liu, M.L. Muolo, F. Valenza, A. Passerone, Survey on wetting of SiC by molten metals, Ceramics Int 36 (2010) 1177–1188.
[37] C.V. Thompson, Solid-State Dewetting of Thin Films, Ann. Rev. Mater. Res. 42 (2012) 399–434.
[38] F. Leroy, L. Borowik, F. Cheynis, Y. Almadori, S. Curiotto, M. Trautmann, J. C. Barbé, P. Müller, How to control solid state dewetting: A short review, Surf. Sci. Rep. 71 (2016) 391–409.
[39] F. Niekiel, P. Schweizer, S.M. Kraschewski, B. Butz, E. Spiecker, The process of solid-state dewetting of Au thin films studied by in situ scanning transmission electron microscopy, Acta Mater 90 (2015) 118–132.
[40] F. Ruffino, M.G. Grimaldi, Self-organized patterned arrays of Au and Ag nanoparticles by thickness-dependent dewetting of template-confined films, J. Mater. Sci. 49 (2014) 5714–5729.
[41] F. Ruffino, M.G. Grimaldi, Nanostructuration of thin metal films by pulsed laser irradiations: a review, Nanomaterials 9 (2019) 1133.
[42] H. Krishna, C. Favazza, A.K. Gangopadhyay, R. Kalyanaraman, Functional Nanostructures through Nanosecond Laser Dewetting of Thin Metal Films, JOM 60 (2008) 37–42.
[43] H. Krishna, R. Sachan, J. Strader, C. Favazza, M. Khenner, R. Kalyanaraman, Thickness-dependent spontaneous dewetting morphology of ultrathin Ag films, Nanotechnology 21 (2010), 155601.
[44] B. Drevet, S. Kalogeropoulou, N. Eustathopoulos, Wettability and interfacial bonding in Au–Si/SiC system, Acta Metall. Mater. 41 (1993) 3119–3126.
[45] Y.V. Naidich, V. Zhuravlev, N. Krasovskaya, The wettability of silicon carbide by Au–Si alloys, Mater. Sci. Eng. A 245 (1998) 293–299.
[46] G. Abadias, L. Simonot, J.J. Colin, A. Michel, S. Camelio, D. Babonneau, Volmer-Weber growth stages of polycrystalline metal films probed by in situ and real-time optical diagnostics, Appl. Phys. Lett. 107 (2015), 183105.
[47] F. Ruffino, M.G. Grimaldi, Island-to-percolation transition during the room-temperature growth of sputtered nanoscale Pd films on hexagonal SiC, J. Appl. Phys. 107 (2010), 074301.
[48] J.A. Venables, Introduction to surface and thin film processes, Cambridge University Press, Cambridge, 2000.
[49] V.K. Kumikov, K.B. Khokonov, On the measurement of surface free energy and surface tension of solid metals, J. Appl. Phys. 54 (1983) 1346–1350.
[50] H.R. Rafiee, A. Boushehri, A general equation for the surface tension of metals based on the law of corresponding states, High Temperatures-High Pressures 34 (2002) 393–400.
[51] H.M. Lu, Q. Jiang, Surface Tension and Its Temperature Coefficient for Liquid Metals, J. Phys. Chem. B 109 (2005) 15463–15468.
[52] F. Aqra, A. Ayyad, Theoretical temperature-dependence surface tension of pure liquid gold, Mater. Lett. 65 (2011) 2124–2126.
[53] F. Aqra, A. Ayyad, Surface energies of metals in both liquid and solid states, Appl. Surf. Sci. 257 (2011) 6372–6379.
[54] S.Dukarov, A.Kryshtal, V.Sukhov, Surface Energy and Wetting in Island Films, in the book "Wetting and Wettability" edited by M.Aliofkhazraei, INTECHOPEN, 2015.
[55] T. Takai, T. Halicioğlu, W.A. Tiller, Reconstruction and energetics for surfaces of silicon, diamond and β-SiC, Surface science 164 (1985) 341–352.
[56] N. Eustathopoulos, M.G. Nicholas, B. Drevet, Wettability at High Temperatures, Pergamon, New York, 1999.
[57] M.B. Cortie, The weird world of nanoscale gold, Gold Bull 37 (2004) 12–19.
[58] R.F. Egerton, Physical Principles of Electron Microscopy, Springer, Switzerland, 2016.

[59] B. Ressel, K.C. Prince, S. Heun, Wetting of Si surfaces by Au-Si liquid alloys, J. Appl. Phys. 93 (2003) 3886–3892.
[60] A. Suzuki, H. Ashida, N. Furui, K. Mameno, H. Matsunami, Thermal oxidation of SiC and electrical properties of Al-SiO_2-SiC MOS structure, Jap. J. Appl. Phys. 21 (1982) 579–585.
[61] H. Kurimoto, K. Shibata, C. Kimura, H. Aoki, T. Sugino, Thermal oxidation temperature dependence of 4H-SiC MOS interface, Appl. Surf. Sci. 253 (2006) 2416–2420.
[62] R.H. Kikuchi, K. Kita, Fabrication of SiO_2/4H-SiC (0001) interfacewith nearly ideal capacitance-voltage characteristics by thermal oxidation, Appl. Phys. Lett. 105 (2014), 032106.
[63] W. Klement, R. Willens, P. Duwez, on-Crystalline Structure in Solidified Gold-Silicon Alloys, Nature 187 (1960) 869–870.
[64] T. Anantharaman, H. Luo, W. Klement, Formation of New Intermediate Phases in Binary Eutectic Systems by Drastic Undercooling of the Melt, Nature 210 (1966) 1040–1041.
[65] M. Censabella, M.G. Grimaldi, F. Ruffino, Shape design of supported Au nanorods through morphological evolution: coalescence, instability, reshaping, Mater. Charact. 147 (2019) 101–115.
[66] A.B. Taylor, A.M. Siddiquee, J.W.M. Chon, Below melting point photothermal reshapingof single gold nanorods driven by surface diffusion, ACS Nano 8 (2014) 12071–12079.
[67] K. Nogi, K. Ogino, Wettability of SiC by liquid pure metals, Trans. Jpn. Inst. Met. 29 (1988) 742–747.